2014 IEEE International Conference on Robotics & Automation (ICRA)
Hong Kong Convention and Exhibition Center
May 31 - June 7, 2014. Hong Kong, China

Modeling and Primary Experiment of a 3-axis PID Control with 50 nm resolution for a Holonomic Precision Inchworm Robot*

M. Yatsurugi, A. Oi, O. Fuchiwaki, *Member, IEEE*, T. Higuchi

Abstract— **In this paper, we describe design and development of a 3-axis proportional-integral-derivative (PID) controller for a holonomic precision inchworm robot. The mechanism has two Y-shaped electromagnets and six piezoelectric actuators (PAs) for obtaining 3-degrees-of-freedom (3DoF) motion on well-polished ferromagnetic surfaces. To measure its 3DoF position simultaneously, an integrated 3DoF inner position sensor composed of 4 linear encoders are developed. In experiments, we have checked that this arrangement of the encoders is valid for measuring the 3DoF motion under a condition without disturbance. To be robust against the disturbance, we also discuss requirement of an acceleration feedforward controller with 3 motion sensors to detect disturbance and slips of supporting electromagnet. This paper is first article which demonstrates simultaneous 3-axis PID control with nanometer-scale positioning resolution of miniature mobile robot driven by PAs. We also discuss about the future direction of the realization of compact, precise, fast, flexible, and energy-efficient mobile robotic factory.**

I. Introduction

Recently, wheeled mobile mechanisms are widely used in transportation robots [1]. In most cases, the mechanisms have various sensors for monitoring their internal state. They have rotary encoders which are attached to their motors to change their moving directions and velocities via controlling rotational speed of wheels. They also have motion sensors for monitoring outer vibrations and disturbance. Recently, MEMS motion sensors are widely attached in various transportation devices, such as smart phones, hard-disks, CCD-cameras, and cars because they are very compact, e.g. 5 x 5 x 1mm; it is easy to attach on them. In most case, the acceleration and angular velocity sensors are packaged into one MEMS chip. An acceleration feedforward (FF) controller with the MEMS motion sensors is widely used to measure outer vibrations for those transportation devices [2, 3]. On the other hand, there are many multi-axial linear stages inside production equipment [4]. In most cases, we use only linear encoders for measuring their position. In most cases, commercially available 3-axial linear stages with 50 cm^2 and 360° of positioning ranges are around 100 kg, although widely-used chip parts are less than 1mg. Because of their heavy-weight, the production equipment requires too much power to carry the tiny parts and brings too large inertia force. That large inertia force generates big vibration around the equipment. To minimize and damp the big vibration, we need to make factory's floors rigid and attach expensive anti-vibration devices. Recently, there are some research activities about miniature precise mobile robots driven by piezoelectric actuators (PAs) [5-10]. They have 3DoF holonomic motion and their weight is less than 100g. That lightweight is very effective for reduction of space and energy. However, it is difficult to attach inner sensors to them because they are very small. That is why their measuring methods are limited to only "outer" sensors thus far, i.e. combination of CCD-camera for global navigation and microscopic image for precise positioning [5, 8]. Visual feedback (FB) method used by microscopic image cannot realize both of wide measuring area and high measurement resolution. If we get high resolution, the measuring area becomes narrow. Besides, when we use only those outer sensors, we cannot control them fast enough to use them high-speed productive applications, such as pick and place of the chip parts. We should add inner sensors to improve their positioning speed and accuracy because the inner sensors have both of high measuring speed and resolution enough to measure outer and inner disturbance in most cases. We also need take into account a disturbance generated by slips of their supporting legs [11, 12]. In previous report, we have described that design of an integrated 3DoF inner position sensor composed of 4 linear encoders to control our holonomic inchworm robot precisely in x, y, and θ axes simultaneously. We have also solved theoretical fastest 2DoF positioning signals under the condition of no disturbance used by bang-bang control method [13]. In this paper, we report about a modeling and primary experiment of a 3-axis simultaneous PID control and discuss further design of dynamical and precise control method by adding the motion sensors. In chapter 2, we summarize the modeling method of our mechanism. In chapter 3, we explain design and measuring principle of the 3DoF inner position sensor. In chapter 4, we demonstrate proportional-integral-derivative (PID) control in 3-axis with 50 nm resolution to check the validity of the developed 3DoF position sensor. This article is first paper showing experimental results of simultaneous 3-axis PID control for the miniature mobile robots with nanometer-scale resolution. In chapter 4, we discuss requirement of the acceleration FF controller with motion sensors to measure external vibration. We also explain arrangement of the motion sensors and how to detect the slips. These contributions are paid for getting higher positioning accuracy of the robot to realize compact, flexible, fast, and precise robotic factory.

*This research had been supported by Adaptable and Seamless Technology Transfer Program through Target-driven R&D (A-Step), FS Exploratory Research.

O. Fuchiwaki is Dept. of Mechanical Engin. with the Yokohama National Univ., 1-79 Tokiwadai, Hodogaya-ku, Yokohama, Kanagawa, Japan (phone: +81-45-339-3693; fax: +81-45-339-3693; e-mail: ohmif@ynu.ac.jp).

M. Yatsurugi is with the Honda Motor Co.

A. Akio is with the Dept. of Mechanical Engineering, Yokohama National University (YNU).

T. Higuchi is Dept. of Ocean Engin. and Ecosystem Science Systems with the Yokohama National Univ., 1-79 Tokiwadai, Hodogaya-ku, Yokohama, Kanagawa, Japan (e-mail: higuchi@ynu.ac.jp).

II. 3DoF INCHWORM MECHANISM

A. Structure and performance

Fig. 1 shows the structure of the mechanism. *EM-1* and *EM-2* are two Y-shaped electromagnets (EMs) that are separate to avoid attracting each other. These Y-shaped EMs make a closed loop via a ferromagnetic surface to obtain enough magnetic force. *PZT-F*, *PZT-B*, *PZT-L1*, *PZT-L2*, *PZT-R1*, and *PZT-R2* are the six PAs. We arrange *EM-1* and *EM-2* to cross each other and connect to the six PAs so that the mechanism can precisely move in any direction by the inchworm principle. Fig. 2 shows a photograph of the mechanism. The mechanism is 100 g, 86 mm in length and width, and 11 mm in height. The mechanism has parallel leaf springs for smooth contact of all the legs on the surface simultaneously. Table 1 shows the typical performance of the mechanism. We used APA50XS "Moonie" PAs (Cedrat Inc.) connected in a series. Table 2 shows the typical performance of the PAs. Fig. 3 shows the motion sequence of orthogonal

TABLE I
PERFORMANCE OF THE INCHWORM MOBILE MECHANISM

Quantity	
Step length (120 V)	0.1~62 μm
Resolution (15-25ºC, Less than 50% rH)	Better than 10 nm
DoF	X,Y, θ
Natural Frequency (blocked free)	500~600 Hz
Maximum Velocity (Frequency)	~5 mm/s (100Hz)
Repeatability (CV; Ratio of SD of positioning error to a path length) (Frequency)	~1% (100Hz)
Thrust force	1.5 N
Pay load	150 g
Height x Thickness x Length	86 x 86 x 15 mm
Weight	100 g

TABLE II
PERFORMANCE OF THE PIEZOELECTRIC ACTUATORS

Quantity	
Displacement (100 V)	95.5 ± 5 μm
Generative Force (100 V)	18.0 N
Spring constant	115,000 N/m
Capacitance	1.04 μF
Resolution (15-25ºC, Less than 50% rH)	1.52 nm
Natural Frequency (blocked free)	1.45 kHz
Height x Thickness x Length	12.9 x 6.4 x 9.2 mm
Weight	4 g

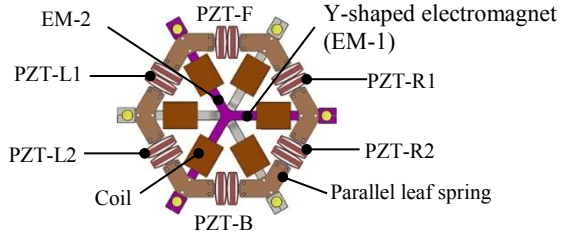

Fig. 1. Structure of the 3DoF inchworm mechanism

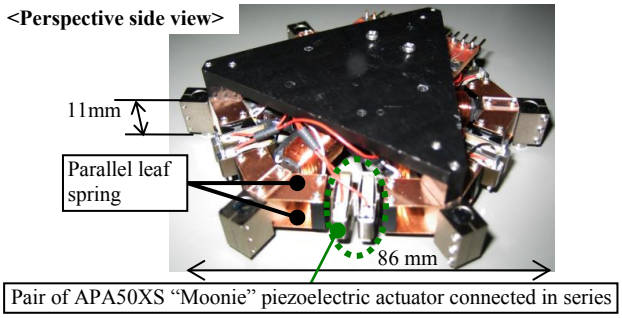

Fig. 2 Photograph of the omnidirectional mechanism

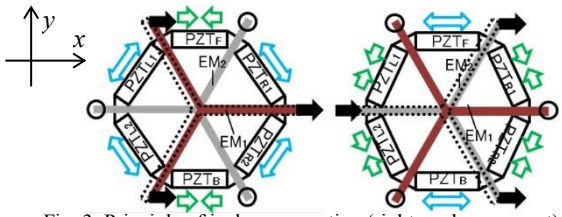

Fig. 3. Principle of inchworm motion (rightward movement)

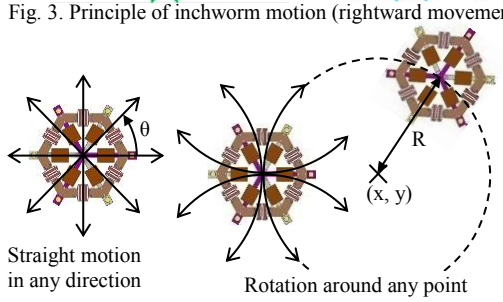

Fig. 4. Motion patterns

motions in the *x*-axis. This mechanism moves like an inchworm while retaining the synchronism among the rectangular-shaped forces of the two EMs and vibrations of the six PAs. This mechanism enables the robot to move precisely in any 3DoF motion with a resolution of better than 10 nm by changing the amplitude of the vibrations. As shown in Fig. 4, the mechanism moves straight in any direction and rotates around any point precisely. This small mechanism moves flexibly and widely on well-polished ferromagnetic surfaces. Note that a minimum step width of the inchworm motion is around 100 nm as shown in Table 1 because of a disturbance generated by switching of the EMs. However, when we keep one EM fixed to the floor, we have checked that the other can be positioned precisely better than 10 nm of the resolution from experiments because the lower limit of the resolution is determined 1.52 nm of the PA's resolution under the condition listed in table 2.

B. 3DoF Dynamic model

As depicted in fig. 5, we define the 3DoF dynamic model of the mechanism when *EM-2* is free and *EM-1* is fixed. Here, k_L and k_S are the spring constants of the six PAs in compression and shear deformations, respectively. c_S is the damping constant of the actuators in shear deformation. d_F is the enforced displacement of the piezoelectric actuator of *PZT-F*, and d_B, d_{R1}, d_{R2}, d_{L1}, and d_{L2} are similarly defined. We assume that *EM-1* and *EM-2* are rigid bodies. *EM-1* and *EM-2* are connected by hinged joints at P_1, P_2, and P_3. O_1, O_2, and O_3 are the initial positions of P_1, P_2, and P_3, respectively. x_1 and y_1 are coordinates of P_1; x_2 and y_2 and x_3, and y_3 similarly define P_2 and P_3, respectively. P_{G1} is the center of gravity of *EM-1*. The position of P_{G1} is represented by an orthogonal coordinate system used by x_{G1} and y_{G1}, and P_{G2} is similarly defined by x_{G2} and y_{G2}. O_{G1} is the origin point of P_{G1}. The six PAs move P_1, P_2, and P_3. 3DoF motion of *EM-2* is determined by the positions of P_1, P_2, and P_3; thus, the PAs move the free leg, *EM-2*. $\overrightarrow{F_r}$ is a frictional force vector acting on *EM-1* from the floor surface. F_x and F_y are coordinates of $\overrightarrow{F_r}$ in the *X*- and *Y*-axes, respectively. N_f is the moment of force acting on *EM-1* from the frictional force. m is defined as each of the mass of *EM-1* and *EM-2*. I is defined as each of the moment of inertia of *EM-1* and *EM-2* about their own gravity centers. r is

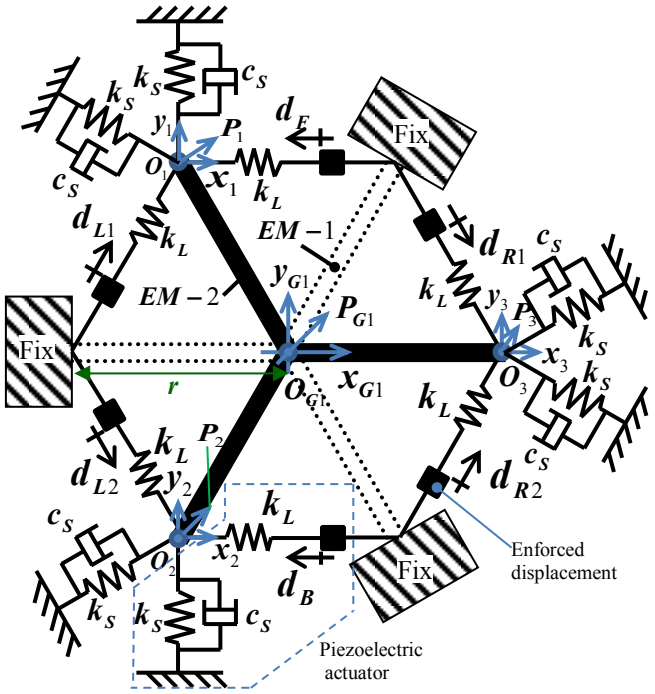

Fig. 5. 3DoF dynamic model

defined as a distance between mechanical center and an end of EM. When EM-1 is in static condition, $\ddot{x}_{G1}$, $\ddot{y}_{G1}$ and $\ddot{\theta}_{G1}$ are 0. From Fig. 5, Newton's equations of motion for *EM-1* and *EM-2* in the *x*-, *y*-, and θ-axes are represented as,

$$\begin{bmatrix} m\ddot{x}_{G1} \\ m\ddot{y}_{G1} \\ I\ddot{\theta}_1 \end{bmatrix} = \begin{bmatrix} 0 \\ 0 \\ 0 \end{bmatrix} = \begin{bmatrix} F_x \\ F_y \\ N_f \end{bmatrix} + 3(k_s + k_L) \begin{bmatrix} x_{G2} \\ y_{G2} \\ \frac{r^2}{2}\theta_2 \end{bmatrix} + 3c_s \begin{bmatrix} \dot{x}_{G2} \\ \dot{y}_{G2} \\ \frac{r^2}{2}\dot{\theta}_2 \end{bmatrix} + k_L \begin{bmatrix} d_F + d_B - \frac{1}{2}(d_{L1} + d_{L2} + d_{R1} + d_{R2}) \\ \frac{\sqrt{3}}{2}(-d_{L1} + d_{L2} + d_{R1} - d_{R2}) \\ \frac{\sqrt{3}}{2}r(-d_F + d_{L1} - d_{L2} + d_B + d_{R1} - d_{R2}) \end{bmatrix}, \quad (1)$$

$$\begin{bmatrix} m\ddot{x}_{G2} \\ m\ddot{y}_{G2} \\ I\ddot{\theta}_2 \end{bmatrix} = -3(k_s + k_L) \begin{bmatrix} x_{G2} \\ y_{G2} \\ \frac{r^2}{2}\theta_2 \end{bmatrix} - 3c_s \begin{bmatrix} \dot{x}_{G2} \\ \dot{y}_{G2} \\ \frac{r^2}{2}\dot{\theta}_2 \end{bmatrix} - k_L \begin{bmatrix} d_F + d_B - \frac{1}{2}(d_{L1} + d_{L2} + d_{R1} + d_{R2}) \\ \frac{\sqrt{3}}{2}(-d_{L1} + d_{L2} + d_{R1} - d_{R2}) \\ \frac{\sqrt{3}}{2}r(-d_F + d_B + d_{L1} - d_{L2} + d_{R1} - d_{R2}) \end{bmatrix}. \quad (2)$$

We define F_{max} as the maximum static frictional force between *EM-1* and the floor surface as given by

$$F_{max} \equiv \mu(mg + F_{ad}). \quad (3)$$

Here, μ is the coefficient of static friction, and F_{ad} is the magnetic force between *EM-1* and the surface. If the supporting leg of *EM-1* is fixed to the surface, the sum of forces on *EM-1* becomes zero, as shown in (1), and the absolute value of $\overrightarrow{F_r}$ requires following condition,

$$\left|\overrightarrow{F_r}\right| = \sqrt{{F_x}^2 + {F_y}^2} \le F_{max}. \quad (4)$$

C. State Space Representation

We assumed that the displacements of the actuators are approximately proportional to their input voltages, which we defined as the proportional coefficient, *h*. Therefore, we can calculate the input voltage to the actuator, *V(t)*, as follows:

$$\boldsymbol{V}(t) \equiv \begin{bmatrix} V_F(t) \\ V_B(t) \\ V_{L1}(t) \\ V_{L2}(t) \\ V_{R1}(t) \\ V_{R2}(t) \end{bmatrix} \equiv h \begin{bmatrix} d_F(t) \\ d_B(t) \\ d_{L1}(t) \\ d_{L2}(t) \\ d_{R1}(t) \\ d_{R2}(t) \end{bmatrix}. \quad (5)$$

We define control variable as $\boldsymbol{u}(t)$, that is input signals generated with a FPGA board (LabVIEW, PCIe-7852R LX50) as given by,

$$\boldsymbol{u}(t) \equiv \begin{bmatrix} u_1(t) \\ u_2(t) \\ u_3(t) \\ u_4(t) \\ u_5(t) \\ u_6(t) \end{bmatrix} \equiv \begin{bmatrix} u_F(t) \\ u_B(t) \\ u_{L1}(t) \\ u_{L2}(t) \\ u_{R1}(t) \\ u_{R2}(t) \end{bmatrix}. \quad (6)$$

$\boldsymbol{u}(t)$ is amplified *j*-fold and added offset voltage of V_0 with an amplifier, then becomes $\boldsymbol{V}(t)$ as,

$$\begin{bmatrix} V_F(t) \\ V_B(t) \\ V_{L1}(t) \\ V_{L2}(t) \\ V_{R1}(t) \\ V_{R2}(t) \end{bmatrix} \equiv j \begin{bmatrix} u_F(t) \\ u_B(t) \\ u_{L1}(t) \\ u_{L2}(t) \\ u_{R1}(t) \\ u_{R2}(t) \end{bmatrix} + V_0 \begin{bmatrix} 1 \\ 1 \\ 1 \\ 1 \\ 1 \\ 1 \end{bmatrix}. \quad (7)$$

From (5) and (7), enforced displacement $\boldsymbol{n}(t)$ is described as,

$$\boldsymbol{n}(t) \equiv \begin{bmatrix} d_F(t) \\ d_B(t) \\ d_{L1}(t) \\ d_{L2}(t) \\ d_{R1}(t) \\ d_{R2}(t) \end{bmatrix} = \frac{j}{h} \begin{bmatrix} u_F(t) \\ u_B(t) \\ u_{L1}(t) \\ u_{L2}(t) \\ u_{R1}(t) \\ u_{R2}(t) \end{bmatrix} + \frac{V_0}{h} \begin{bmatrix} 1 \\ 1 \\ 1 \\ 1 \\ 1 \\ 1 \end{bmatrix}. \quad (8)$$

By substituting (8) into (2),

$$\dot{\boldsymbol{x}}(t) = \boldsymbol{A}\boldsymbol{x}(t) + \boldsymbol{B}\boldsymbol{u}(t). \quad (9)$$

(9) represents a state equation of the mechanism. Note that offset enforced displacement V_0/h in (8) becomes *0* in (9) because 6 PAs cancel each other's offset displacements out. We define $\boldsymbol{x}(t)$ and $\boldsymbol{y}(t)$ as state and control variables respectively. $\boldsymbol{A}$ and $\boldsymbol{B}$ are also defined as follows,

$$\boldsymbol{x}(t) \equiv \begin{bmatrix} x_1(t) \\ x_2(t) \\ x_3(t) \\ x_4(t) \\ x_5(t) \\ x_6(t) \end{bmatrix} \equiv \begin{bmatrix} x_{G2}(t) \\ y_{G2}(t) \\ \theta_{G2}(t) \\ \dot{x}_{G2}(t) \\ \dot{y}_{G2}(t) \\ \dot{\theta}_2(t) \end{bmatrix} \equiv \begin{bmatrix} x_G(t) \\ y_G(t) \\ \theta(t) \\ \dot{x}_G(t) \\ \dot{y}_G(t) \\ \dot{\theta}(t) \end{bmatrix}, \quad (10)$$

$$\boldsymbol{y}(t) \equiv \begin{bmatrix} x_1(t) \\ x_2(t) \\ x_3(t) \end{bmatrix}, \quad (11)$$

$$\boldsymbol{A} \equiv \begin{bmatrix} 0 & 0 & 0 & 1 & 0 & 0 \\ 0 & 0 & 0 & 0 & 1 & 0 \\ 0 & 0 & 0 & 0 & 0 & 1 \\ \frac{-3(k_s + k_L)}{m} & 0 & 0 & \frac{-3c_s}{m} & 0 & 0 \\ 0 & \frac{-3(k_s + k_L)}{m} & 0 & 0 & \frac{-3c_s}{m} & 0 \\ 0 & 0 & \frac{-3(k_s + 3k_L)r^2}{2I} & 0 & 0 & \frac{-3c_s r^2}{2I} \end{bmatrix}, \quad (12)$$

$$\boldsymbol{B} \equiv \frac{k_L j}{h}\begin{bmatrix} 0 & 0 & 0 & 0 & 0 & 0 \\ 0 & 0 & 0 & 0 & 0 & 0 \\ 0 & 0 & 0 & 0 & 0 & 0 \\ \frac{-1}{m} & \frac{-1}{m} & \frac{1}{2m} & \frac{1}{2m} & \frac{1}{2m} & \frac{1}{2m} \\ 0 & 0 & \frac{\sqrt{3}}{2m} & -\frac{\sqrt{3}}{2m} & -\frac{\sqrt{3}}{2m} & \frac{\sqrt{3}}{2m} \\ \frac{1}{I} & \frac{-1}{I} & \frac{-1}{I} & \frac{1}{I} & \frac{-1}{I} & \frac{1}{I} \end{bmatrix}. \quad (13)$$

Output equation is represented by,

$$\boldsymbol{y}(t) = \boldsymbol{C}\boldsymbol{x}(t) \quad (14)$$

Here, $\boldsymbol{C}$ is defined as given by,

$$\boldsymbol{C} \equiv \begin{bmatrix} 1 & 0 & 0 & 0 & 0 & 0 \\ 0 & 1 & 0 & 0 & 0 & 0 \\ 0 & 0 & 1 & 0 & 0 & 0 \end{bmatrix}. \quad (15)$$

Because (15) does not have control variable of $\boldsymbol{u}(t)$, the proposed dynamical model is strictly proper. When we define initial value of state variables as $\boldsymbol{x}(0)$ and we take Laplace transform in (9) and (14), we can obtain these transfer function matrices of $P_U(s)$ and $P_0(s)$ as given by,

$$\boldsymbol{P_U}(s) \equiv \boldsymbol{C}(s\boldsymbol{I}(s) - \boldsymbol{A})^{-1}\boldsymbol{B} \quad (16)$$

$$\boldsymbol{P_0}(s) \equiv \boldsymbol{C}(s\boldsymbol{I}(s) - \boldsymbol{A})^{-1} \quad (17)$$

$$\boldsymbol{Y}(s) = \boldsymbol{P_U}(s)\boldsymbol{U}(s) + \boldsymbol{P_0}(s)\boldsymbol{x}(0). \quad (18)$$

We omit the detailed representation of $P_U(s)$ and $P_0(s)$ due to limitations of space. Here, we define Laplace transform of $\boldsymbol{x}(t)$ as $\boldsymbol{X}(s)$. Laplace transform of other parameters is defined in a similar way. If we define $\boldsymbol{d}(t)$ as disturbance including outer vibration, block diagram representation of (18) as open loop control is shown in fig. 6.

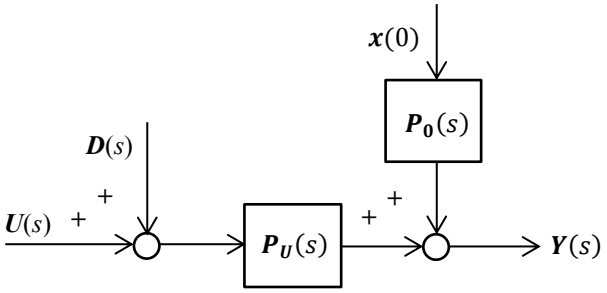

Fig. 6. Block diagram with open-loop control

III. Integrated 3DoF Inner Position Sensor

A. Design

In Fig. 7, we show the design of an integrated 3DoF inner position sensor with four optical chip encoders (Mercury1540P, MicroE systems). These chip encoders have 0.5μm resolution and a maximum measuring speed of 7.2m/s as listed in Table 3. These encoders measure the displacement of a sinusoidal vibration up to 120 kHz with its maximum amplitude of 100μm. Four chip encoders are fixed to EM-2, and their scales are fixed to EM-1. If one EM is fixed to the floor, the other's motion is measured by the four encoders in the x-, y-, and θ-axes with 0.5μm resolution.

B. Conversion of Measured Values to Control Variables

We explained the measuring principle of the integrated 3DoF inner position sensor in previous report [13], so we omit the detailed explanation and describe the outline. We define Δx, Δy, and $\Delta\theta$ as measured displacement of the sensor.

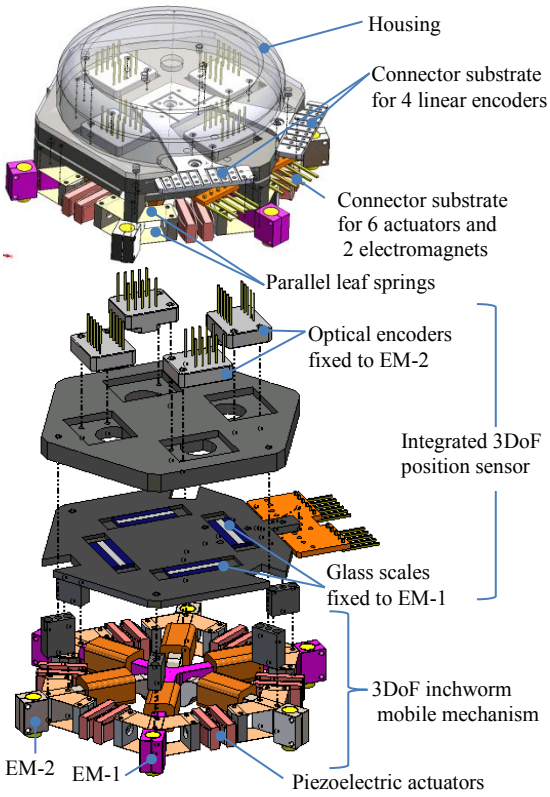

Fig. 7. Assembly drawing

TABLE III
Performance of the Chip Encoder

Quantity	
Resolution	0.5 μm/count
Maximum measuring speed	7200 mm/s
Height x Thickness x Length	12.7 x 15.2 x 5.6 mm
Weight	2.6 g

To simplify the problem, we approximates $\Delta\theta \ll 1$. Note that Δx, Δy, and $\Delta\theta$ are relative displacements between EMs. When we define four measured values of four encoders as Y_1, X_2, Y_3, and X_4. Δx, Δy, and $\Delta\theta$ are represented by,

$$\begin{bmatrix} \Delta x(t) \\ \Delta y(t) \\ \Delta\theta(t) \end{bmatrix} \approx \pm \boldsymbol{F}\boldsymbol{z}(t). \quad (19)$$

$$\boldsymbol{z}(t) \equiv \begin{bmatrix} Y_1(t) \\ X_2(t) \\ Y_3(t) \\ X_4(t) \end{bmatrix} \quad (20)$$

$$\boldsymbol{F} \equiv \begin{bmatrix} 0 & \frac{1}{2} & 0 & \frac{1}{2} \\ \frac{1}{2} & 0 & \frac{1}{2} & 0 \\ \frac{1}{4r} & -\frac{1}{4r} & -\frac{1}{4r} & \frac{1}{4r} \end{bmatrix} \quad (21)$$

$$Y_1(t) + X_2(t) + Y_3(t) + X_4(t) = 0 \quad (22)$$

When EM-1 with the scales is fixed and the EM-2 with the encoders is movable, ± of sign in (19) is plus. Conversely, the EM-2 is fixed and EM-1 is movable, the sign is minus. Note that $\Delta\theta$ is represented as best estimator,

$$\Delta\theta(t) \equiv \tfrac{1}{2}(\Delta\theta_1(t) + \Delta\theta_2(t)), \quad (23)$$

because $\Delta\theta(t)$ can be calculated by the following two equations,

$$\Delta\theta_1(t) \equiv \frac{1}{2r}(Y_1 - Y_3), \tag{24}$$

$$\Delta\theta_2(t) \equiv \frac{1}{2r}(-X_2 + X_4). \tag{25}$$

(22) represents relationship among Y_1, X_2, Y_3, and X_4. Because 3DoF of the mechanism is measured by four encoders, there must be one relationship among four measured values of (22). If there are no outer vibrations and disturbance, fixed EM and the floor are completely resting state on a coordinate system at rest. Under that ideal condition and when *EM-1* is fixed, control variables equal to Δx, Δy, and $\Delta\theta$ as given by,

$$\boldsymbol{y}(t) \equiv \begin{bmatrix} x_1(t) \\ x_2(t) \\ x_3(t) \end{bmatrix} = \begin{bmatrix} x_{G2}(t) \\ y_{G2}(t) \\ \theta_{G2}(t) \end{bmatrix} = \begin{bmatrix} \Delta x(t) \\ \Delta y(t) \\ \Delta\theta(t) \end{bmatrix}. \tag{26}$$

$$\boldsymbol{y}(t) = \boldsymbol{F}\boldsymbol{z}(t) \tag{27}$$

IV. 3-AXIS PID CONTROL

A. Experimental setup

To confirm the feasibility of the proposed integrated 3DoF inner position sensor, we developed 3DoF "outer" position sensor which has better measurement resolution of 0.05μm than that of the inner sensors with the same arrangement of the encoders as shown in Figs. 8 and 9. In this experiment, we measured the displacement of the free leg with optical linear encoders (MicroE Systems Inc., Mercury3500) fixed to a working table. Here, glass scales were placed on the housing attached to the free EM. Both of the fixed EM and encoders were clamped to the working table with screws. In this setup, we measured displacements of the free EM in x, y, and θ-axis. Input signals were generated with the FPGA board (LabVIEW, PCIe-7852R) and amplified 32-fold with an amplifier. Fig 10 shows the block diagram of 3-axis PID control. $\boldsymbol{k_I}$, $\boldsymbol{k_P}$, and $\boldsymbol{k_D}$ are vectors composed of integral , proportional, and derivative gains in x-, y-, and θ-axis respectively as defined by,

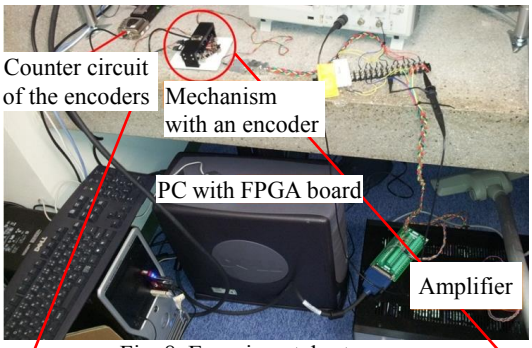

Fig. 8. Experimental setup

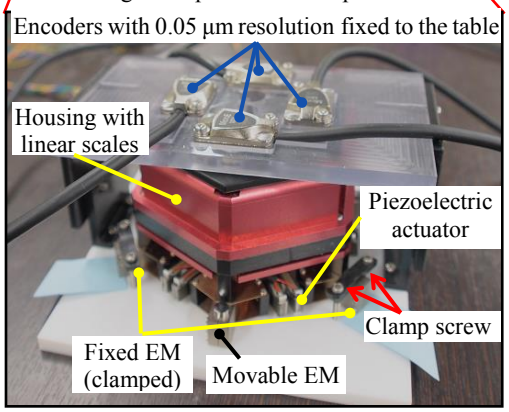

Fig. 9. Close up view of the mechanism with "outer" encoders

$$\boldsymbol{k_I} \equiv [k_{Ix} \quad k_{Iy} \quad k_{I\theta}], \tag{28}$$

$$\boldsymbol{k_P} \equiv [k_{Px} \quad k_{Py} \quad k_{P\theta}], \tag{29}$$

$$\boldsymbol{k_D} \equiv [k_{Dx} \quad k_{Dy} \quad k_{D\theta}]. \tag{30}$$

From (28), (29), and (30), PID controller of $\boldsymbol{C_{PID}}$ is defined as,

$$\boldsymbol{C_{PID}}(s) \equiv \begin{bmatrix} \boldsymbol{k_I}/\boldsymbol{s} \\ \boldsymbol{k_P} \\ \boldsymbol{sk_D} \end{bmatrix} = \begin{bmatrix} k_{Ix}/s & k_{Iy}/s & k_{I\theta}/s \\ k_{Px} & k_{Py} & k_{P\theta} \\ sk_{Dx} & sk_{Dy} & sk_{D\theta} \end{bmatrix}. \tag{31}$$

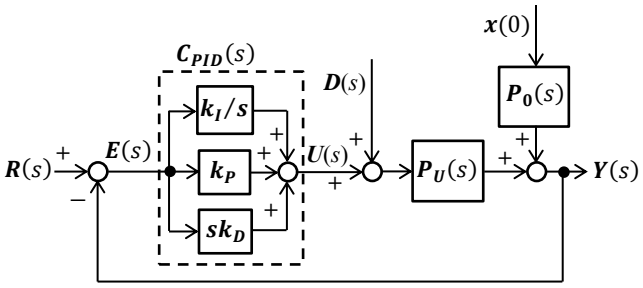

Fig. 10. Block diagram of 3-axis PID control

Table IV
Parameters

Symbol	Parameter	Quantity Average (± σ)
m	Mass of electromagnet (EM)	0.045 [kg]
r	Radius of EM	39 [mm]
k_S	Spring constant of the actuators in shear deformation	Negligibly Small
k_L	Spring constant of the actuators in compression deformation	115000 [N/m]
c_S	Damping constant of the actuators in shear deformation	5.5 ± 0.93 [Ns/m]
h	Proportional coefficient of the actuator	-1.02 [V/μm]
j	Magnification of an amplitude	32
V_O	Offset voltage	50 [V]
F_{ad}	Electromagnetic force	14.1[N]

B. Experimental results

As shown in Figs. 2 and 9, we use the mechanical amplifier to the actuators; there are many springs in the mechanism. These springs easily generate non-negligible vibrations. We checked the theoretical fastest signal obtained by the bang-bang control method was good for decreasing the overshoot and the residual vibration. We succeeded to decrease the overshoot less than 1μm, although the average settling time is 280ms when target displacement is 10μm in x axis as previous papers [13]. Here, the settling time is determined as time that elapses before the positioning error damps within ±2% of the target displacement. However, it is impossible to eliminate the residual vibration completely especially under sub-μm scale because there are numerous non-linear effects such as a thermal drift and a hysteresis of the actuators. PID control is good for reducing the residual vibration and the non-linear effects after the bang-bang control. In this paper, we show primary experimental results of the pure 3-axis PID control to check that control variables are definitely converge when measurement resolution of encoders are ± 0.05μm. Table 4 shows parameters in experiments. We set the measurement and feedback periods

as 15μs. The mechanical resonance period is around 2ms, so we assume that the feedback period is sufficiently small. Note that the overshoots are harmful for delicate precise processing because tiny samples might be easily collapsed. We obtained k_I, k_P, and k_D by a limit sensitivity method (LSM) for single axis PID control of each of x-, y-, and θ-axis as listed in table 5 when there are no overshoot. Fig. 11 shows typical plot of the displacement in x-axis vs. time. When we conduct a 2-axis PID control, we set the target displacement to 10 ± 0.05μm in both of x- and y-axes. When we set their gains to the same gains of the single axis PID control, the two displacements in x- and y- axis did not surely converge by coupling effect between x- and y- axis. However, we found out the two displacements surely converge by random search around the gains of the single axis PID control as listed in table 6. Fig. 12 shows typical plot of the displacements in x and y- axis vs. time. The average settling time is around 40ms in the 2-axis PID control. When we conduct a 3-axis PID control, we set the target displacement to 10 ± 0.05μm in both of x- and y-axes, 0 ± 10^{-6}rad in θ axis. When we set their gains to same gains of the single axis PID control as listed in table 5, the three displacements also did not converge by coupling effect among them. When we set their gains to a combination of the same gains of the 2-axis PID control in table 6 and that of the single axis PID control in θ-axis in table 5 as listed in table 7, we found out that the three displacements surely converge. Fig. 13 shows typical plot of three displacements vs. time. The average settling time is around 95ms in the 3-axis PID control. However, we also check that if we change the target displacements, 3 displacements did not accurately converge when we set the gains as table 7. We concluded that we need to investigate more detailed procedure how to set the PID gains due to the three target displacements. As shown in Fig. 14, we also plan to combine the bang-bang control and this 3-axis PID control to eliminate the overshoots and decrease the settling time as much as possible.

Table V
Minimum settling time without overshoot in single axis PID control and gains obtained by limit sensitivity method

Symbol	Quantity	Target	Settling time Target ± 2%
k_{Ix}	5.64	x=15 ± 0.05μm	12.5 [ms]
k_{Px}	0.08		
k_{Dx}	125		
k_{Iy}	2	y=15 ± 0.05μm	19.5 [ms]
k_{Py}	0.145		
k_{Dy}	125		
$k_{I\theta}$	0.1	θ=0.001 ±10^{-6}rad	8.75 [ms]
$k_{P\theta}$	0.018		
$k_{D\theta}$	50		

Table VI
Minimum settling time and gains without overshoot in 2-axis PID control

Symbol	Quantity	Target	Settling time Target ± 2%
k_{Ix}	2	x=10 ± 0.05μm y=10 ± 0.05μm	40 [ms]
k_{Px}	0.04		
k_{Dx}	125		
k_{Iy}	2		
k_{Py}	0.04		
k_{Dy}	125		

Table VII
Minimum settling time and gains without overshoot in 3-axis PID control

Symbol	Quantity	Target	Settling time Target ± 2%
k_{Ix}	2	x=10 ± 0.05μm y=10 ± 0.05μm θ=0 ±10^{-6}rad	95.3 [ms]
k_{Px}	0.04		
k_{Dx}	125		
k_{Iy}	2		
k_{Py}	0.04		
k_{Dy}	125		
$k_{I\theta}$	0.1		
$k_{P\theta}$	0.018		
$k_{D\theta}$	50		

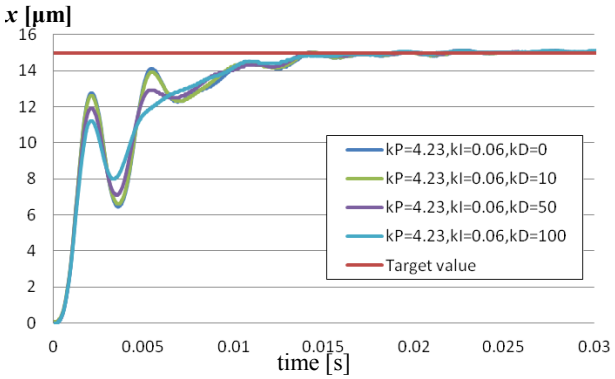

Fig. 11. Plot of x vs. time with 1-axis PID control

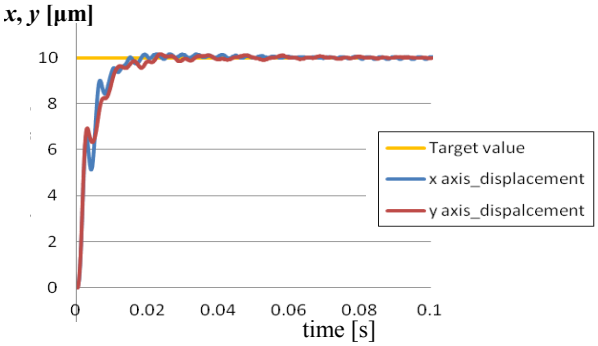

Fig. 12. Plot of x and y vs. time of 2-axis PID control

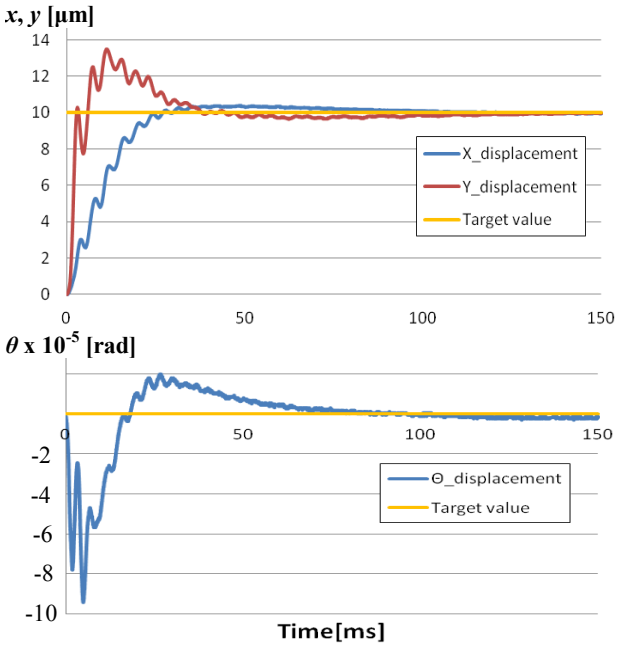

Fig. 13. Plot of displacements vs. time of 3-axis PID control

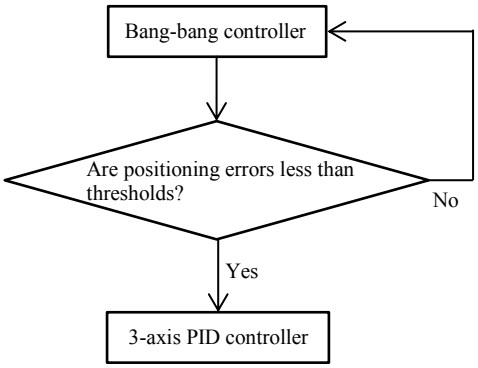

Fig. 14. Flow chart of a bang-bang control and 3-axis PID control

V. Requirement of Acceleration FF Controller

In previous sections, we have explained that the combination of the bang-bang control signals and 3-axis PID controller is one possible approach to achieve fast and precise positioning. However, we still have to consider about an influence of disturbance and slips of the fixed EM because the 3DoF inner position sensor in fig. 7 can only measure relative motions between EMs. Fig. 15 shows simplified 1-axis model with 3 motion sensors, we attach the sensors to each EM and the table. To simplify the explanation, we neglect the influence of rotational accelerations. We can detect the slips of the fixed EM when following condition becomes not true,

$$\boldsymbol{a}_{G1} \equiv \begin{bmatrix} \ddot{x}_{G1}(t) \\ \ddot{y}_{G1}(t) \end{bmatrix} = \begin{bmatrix} \ddot{x}_S(t) \\ \ddot{y}_S(t) \end{bmatrix} \equiv \boldsymbol{a}_S \tag{32}$$

If EM-1 is oscillated by $\boldsymbol{a}_S$, Newton's equation of motion (2) becomes as given by,

$$m\boldsymbol{a}_{G2} = -3(k_s + k_L)\iint (\boldsymbol{a}_{G2} - \boldsymbol{a}_{G1})dt - 3c_s \int (\boldsymbol{a}_{G2} - \boldsymbol{a}_{G1})dt - k_L \begin{bmatrix} 1 & 1 & -\frac{1}{2} & -\frac{1}{2} & -\frac{1}{2} & -\frac{1}{2} \\ 0 & 0 & -\frac{\sqrt{3}}{2} & \frac{\sqrt{3}}{2} & \frac{\sqrt{3}}{2} & -\frac{\sqrt{3}}{2} \end{bmatrix} \boldsymbol{n}(t). \tag{33}$$

We can obtain an inertia force of $\boldsymbol{F_I}$ generated by $\boldsymbol{a}_S$ from the comparison between (2) and (33) as given by,

$$\boldsymbol{F}_I \equiv \begin{bmatrix} F_{S\_x} \\ F_{S\_y} \end{bmatrix} \equiv 3(k_s + k_L)\iint \boldsymbol{a}_{G1}dt + 3c_s \int \boldsymbol{a}_{G1}dt. \tag{34}$$

If we apply additional enforced displacements of $\Delta\boldsymbol{n}(t)$ in (33) to be against $\boldsymbol{F_I}$, the influence of the disturbance is canceled.

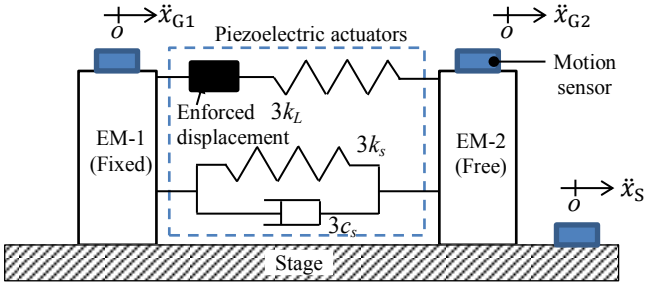

Fig. 15. Arrangement of 3 motion sensors attached on 1-DOF model

VI. Conclusion

We explain requirement to measure an inner state by an inner sensors for miniature mobile robots driven by PAs to obtain precise and fastest control at the beginning. We summarize modeling and principle of the robot and a 3DoF position sensor with four linear encoders. We describe design, development and experimental results of the pure 3-axis PID control to check that x, y, and θ-axes of movable EM are surely converge when measurement resolution of encoders are ± 0.05μm. We achieve settling time of 95ms with 3-axis PID control. We also achieve that of 20ms in 1-axis PID control in each axis. To detect outer vibration which the 3DoF position sensor cannot detect, we explain requirement of an acceleration FF controller with 3 motion sensors. Main contribution of this article is demonstration of simultaneous 3-axis PID control of the miniature mobile robots driven by PAs with nanometer-scale resolution. This paper also contributes to discussion about elimination of influence from outer vibration by acceleration FF controller with 3 motion sensors. We are now developing combination of the bang-bang control and 3-axis PID control with the acceleration FF controller to get more accurate and faster positioning for the miniature mobile robot. Final goal of this project is making precise, fast, flexible, energy-efficient, and compact robotic factory organized by these precise miniature robots for chip mounting and bio-medical applications.

References

[1] T. Braeunl, Embedded Robotics, Mobile Robot Design and Applications with Embedded Systems, Springer Berlin Heidelberg 3rd, ISBN-13 978-3540705338, 2008

[2] M. S. Kang and W. H. Yoon, Acceleration feedforward control in active magnetic bearing system subject to base motion by filtered-X LMS algorithm, IEEE Transactions on Control Systems Technology, Vol. 14, No. 1, pp. 134-140, 2006

[3] A. Jinzenji, et al., Acceleration feedforward control against rotational disturbance in hard disk drives, IEEE Tran. on Magnetics, Vol. 37, No. 2, pp. 888-893, 2001

[4] R. L. Tousain, et al., Fixed structure feedforward controller design exploiting iterative trials: Application to a wafer stage and a desktop printer, J. of Dynamic Systems, Measurement, Vol. 130, No. 5, p. 051006-1/16, 2008

[5] U. Simu, et al., Fabrication of monolithic piezoelectric drive units for a miniature robot, J. Micromech. Microeng., Vol. 12, No. 582, 2002

[6] A. Kortschack, et al., "Driving principles of Mobile Microrobots for the Micro- and Nanohandling", IEEE IROS2003, pp.1895-1900, 2003.

[7] A. Bergander, et al., "Mobile cm^3-microrobots with tools for Nanoscale imaging and micromanipulation" Mechatronics & Robotics (MechRob 2004), pp.1041-1047, 13-15, 2004.

[8] S. Fatikow, et al., "Microrobot system for automatic nanohandling inside a scanning electron microscope", IEEE/ASME T Mech., 12(3), pp.244-252, 2007.

[9] M. Rakotondrabe, et al., 'Development, Modeling, and Control of a Micro-/Nanopositioning 2-DOF Stick Slip Device', IEEE/ASME TMech, 14(6), 2009.

[10] F. Schmoeckel, et al., Smart flexible microrobots for scanning electron microscope (SEM) applications, Proc. of SPIE 3985, Smart Structures and Materials: Smart Structures and Integrated Systems, 142, 2000

[11] O. Fuchiwaki, Insect-sized Holonomic Robots for Precise, Omnidirectional, and Flexible Microscopic Processing: Identification, Design, Development, and Basic Experiments, Precision Engineering, Vol. 37, No. 1, pp. 88-106, 2013

[12] O. Fuchiwaki, et al., Development of 3 DOF Inchworm Mechanism for Flexible, Compact, Low-Inertia, and Omnidirectional Precise Positioning : Dynamical analysis and improvement of maximum velocity within no slip of electromagnets, IEEE/ASME TMech, Vol. 17, No. 4, pp. 697-708, 2012

[13] O. Fuchiwaki, et al., Design of an Integrated 3DoF Inner Position Sensor and 2DoF Feedforward Control for a 3DoF Precision Inchworm Mechanism, Proc. of IEEE ICRA2013, pp. 5475-5481, 2013